Optical Properties of Inverse Opal Photonic Crystals

Rick C. Schroden, Mohammed Al-Daous, Christopher F. Blanford, and Andreas Stein*

Department of Chemistry, University of Minnesota, Minneapolis, Minnesota 55455

Received February 28, 2002. Revised Manuscript Received May 7, 2002

Colloidal crystal-templating methods have been used to prepare inverse opal photonic crystals of silica, mercaptopropyl-functionalized silica, titania, and zirconia. Ordered arrays of uniformly sized polymer spheres were infiltrated with fluid precursors capable of condensation or crystallization. After solidification of the material in the void spaces between the spheres, the polymer templates were removed by calcination or solvent extraction, leaving inverse replicas of the template arrays. By carefully controlling the synthetic procedures, gram-scale quantities of powdered macroporous materials exhibiting photonic crystal properties were obtained. For materials with crystalline walls (titania and zirconia), this required minimization of the size of the nanocrystalline grains. Because the periodicity introduced into the wall structure by the colloidal crystal templates was on the order of optical wavelengths, Bragg diffractions from the planes produced photonic stop bands in the visible spectra of these materials. The stop bands were manifested as brightly colored reflections and an optical filtering behavior of the materials. A crystallographic indexing of the optical spectrum of a polycrystalline inverse opal confirmed the fcc ordering of the pores. The optical properties of these materials were modified in predictable manners by numerous methods, including tailoring the pore size, filling the pores with fluids of various refractive indices, and changing the compositions of the solid material. The wavelengths of the colorful reflections (stop bands) were found to be proportional to the pore size and to vary linearly with the refractive index of the fluid filling the pores. The physical and synthetic modifications reported here allowed for the preparation of powders with optical reflections and bright colors spanning the entire visible spectrum.

Introduction

Since the introduction of the photonic band gap concept,[1,2] the creation of materials exhibiting a three-dimensional periodic modulation of the dielectric constant has been a very active area of research. Such materials, known as photonic crystals, diffract photons from a lattice of dielectric planes in a manner analogous to the behavior of electrons with respect to an atomic crystal lattice.[3] When the refractive index of the dielectric material is sufficiently large, a complete photonic band gap is formed in which Bragg diffractions inhibit a range of wavelengths from propagating through the photonic crystal over all directions.[3−5] Materials exhibiting a complete photonic band gap could provide a number of unique technological applications, including optical waveguides with sharp bends,[6,7] optical integrated circuits,[7] single-mode light-emitting diodes,[3] and low-threshold telecommunications lasers.[1,8,9] Photonic crystals made of dielectric materials with lower refractive indices have an incomplete band gap, yet still exhibit very unique optical properties. Natural examples of photonic crystals with incomplete band gaps include opals that, despite being composed of the optically transparent silica, exhibit a bright display of colors. This variety of photonic crystal, with an incomplete photonic band gap, exhibits stop bands over which selected wavelengths of light are partially inhibited from propagating through the material in certain directions.

Several strategies have been used for the creation of three-dimensional photonic crystals, including the chemical methods of colloidal self-assembly[10−15] and colloidal crystal templating,[16−22] the microfabrication techniques

* To whom correspondence should be addressed.

(1) Yablonovitch, E. *Phys. Rev. Lett.* **1987**, *58*, 2059−2062.
(2) John, S. *Phys. Rev. Lett.* **1987**, *58*, 2486−2489.
(3) Yablonovitch, E. *J. Opt. Soc. Am. B* **1993**, *10*, 283−295.
(4) Joannopoulos, J. D.; Villeneuve, P. R.; Fan, S. *Nature* **1997**, *386*, 143−149.
(5) Special Issue on Electromagnetic Crystal Structures, Design, Synthesis, and Application. *J. Lightwave Technol.* **1999**, *17*.
(6) Mekis, A.; Chen, J. C.; Kurland, I.; Fan, S.; Villeneuve, P. R.; Joannopoulos, J. D. *Phys. Rev. Lett.* **1996**, *77*, 3787−3790.
(7) Lin, S.-Y.; Chow, E.; Hietala, V.; Villeneuve, P. R.; Joannopoulos, J. D. *Science* **1998**, *282*, 274−276.
(8) Yamamoto, Y.; Slusher, R. E. *Phys. Today* **1993**, *46*, 66−73.
(9) John, S. Theory of photonic band gap materials. In *Photonic Band Gap Materials*; Soukoulis, C. M., Ed.; Kluwer Academic Publishers: Dordrecht, The Netherlands, 1996; pp 563−665.
(10) Bogomolov, V. N.; Gaponenko, S. V.; Kapitonov, A. M.; Prokofiev, A. V.; Ponyavina, A. N.; Silvanovich, N. I.; Samoilovich, S. M. *Appl. Phys. A* **1996**, *63*, 613−616.
(11) Bogomolov, V. N.; Gaponenko, S. V.; Germanenko, I. N.; Kapitonov, A. M.; Petrov, E. P.; Gaponenko, N. V.; Prokofiev, A. V.; Ponyavina, A. N.; Silvanovich, N. I.; Samoilovich, S. M. *Phys. Rev. E* **1997**, *55*, 7619−7625.
(12) Mayoral, R.; Requena, J.; Moya, J. S.; López, C.; Cintas, A.; Míguez, H.; Meseguer, F.; Vázquez, L.; Holgado, M.; Blanco, A. *Adv. Mater.* **1997**, *9*, 257−260.
(13) Míguez, H.; López, C.; Meseguer, F.; Blanco, A.; Vázquez, L.; Mayoral, R.; Ocaña, M.; Fornés, V.; Mifsud, A. *Appl. Phys. Lett.* **1997**, *71*, 1148.
(14) Romanov, S. G.; Johnson, N. P.; Fokin, A. V.; Butko, V. Y.; Yates, H. M.; Pemble, M. E.; Sotomayor Torres, C. M. *Appl. Phys. Lett.* **1997**, *70*, 2091.

10.1021/cm020100z CCC: $22.00 © 2002 American Chemical Society
Published on Web 06/26/2002

of mechanically drilling holes within a dielectric slab[23] or stacking logs of a dielectric material,[24−26] and holographic patterning using multiple laser beams.[27] The colloidal crystal-templating approach utilizes the natural tendency of monodisperse spherical particles to self-assemble into a close-packed, or opal, arrangement.[28] The process of filling the voids of the synthetic opal template with a precursor capable of solidification and then removing the template yields a macroporous inverse opal material with a close-packed arrangement of air spheres. The benefit of this self-assembly approach to the fabrication of three-dimensional photonic crystals is the ease with which a dielectric material can be rapidly ordered in three dimensions, compared to the stepwise manner of microfabrication techniques. Variations of the colloidal crystal-templating approach have been used to prepare three-dimensionally ordered macroporous (3DOM) materials with diverse compositions,[22,29] including metal oxides,[16−19,21,30−33] metals,[34−39] semiconductors,[20,40−42] polymers,[43−46] carbons,[47,48] and hybrid organosilicates.[19] Inverse opal materials have been demonstrated to exhibit photonic crystal properties, such as the presence of optical stop bands,[18] tunable color changes,[49] and inhibition of the spontaneous emission of luminescent species intrinsic to or embedded within the photonic crystal.[50−53]

In the current study, poly(methyl methacrylate) (PMMA) colloidal crystal-templating methods were used for the preparation of 3DOM silica, titania, and zirconia, and polystyrene (PS) colloidal crystal templates were used for mercaptopropyl-functionalized silica. The materials were prepared by infiltration of the precursor solution through a powdered colloidal crystal template, using a salt solution for the preparation of 3DOM zirconia and sol−gel precursors for the other compositions. The syntheses were optimized for each composition, with careful attention being paid to the choice of precursor and template removal conditions, to produce materials with photonic crystal properties. Using the technique of templating with a powdered PMMA colloidal crystal, the photonic crystals produced had random orientations of crystal planes throughout the materials. As a result, the apparent colors of the bulk macroporous samples were not angle-dependent. Instead, through the choice of appropriate synthetic procedures, bright and relatively uniformly colored materials could be produced. These materials exhibited optical properties that could be modified by changing a number of factors, including the composition of the wall material, the spacing of the pores, the solid fraction of the material, and the refractive indices of the walls and the void-filling material. Processes for modifying the optical properties of colloidal crystals and inverse opals have previously been reported and modeled[45,54−56] for materials that respond to thermal or chemical changes,[57−61] infiltration with solvents,[10,11,49,62] application of an electric field to liquid crystal-filled materi-

(15) Vlasov, Y. A.; Astratov, V. N.; Karimov, O. Z.; Kaplyanskii, A. A.; Bogomolov, V. N.; Prokofiev, A. V. *Phys. Rev. B* **1997**, *55*, R13357−R13360.
(16) Velev, O. D.; Jede, T. A.; Lobo, R. F.; Lenhoff, A. M. *Nature* **1997**, *389*, 447−448.
(17) Holland, B. T.; Blanford, C. F.; Stein, A. *Science* **1998**, *281*, 538−540.
(18) Wijnhoven, J. E. G. J.; Vos, W. L. *Science* **1998**, *281*, 802−804.
(19) Holland, B. T.; Blanford, C. F.; Do, T.; Stein, A. *Chem. Mater.* **1999**, *11*, 795−805.
(20) Blanco, A.; Chomski, E.; Grabtchak, S.; Ibisate, M.; John, S.; Leonard, S. W.; Lopez, C.; Meseguer, F.; Miguez, H.; Mondia, J. P.; Ozin, G. A.; Toader, O.; van Driel, H. M. *Nature* **2000**, *405*, 437−440.
(21) Yan, H.; Blanford, C. F.; Holland, B. T.; Smyrl, W. H.; Stein, A. *Chem. Mater.* **2000**, *12*, 1134−1141.
(22) Special Issue on Photonic Crystals. *Adv. Mater.* **2001**, *13*.
(23) Yablonovitch, E.; Gmitter, T. J.; Leung, K. M. *Phys. Rev. Lett.* **1991**, *67*, 2295.
(24) Ho, K.; Chan, C.; Soukoulis, C.; Biswas, R.; Sigalas, M. *Solid State Commun.* **1994**, *89*, 413−416.
(25) Sözüer, H.; Dowling, J. *J. Mod. Opt.* **1994**, *41*, 231−239.
(26) Lin, S. Y.; Fleming, J. G.; Hetherington, D. L.; Smith, B. K.; Biswas, R.; Ho, K. M.; Sigalas, M. M.; Zubrzycki, W.; Kurtz, S. R.; Bur, J. *Nature* **1998**, *394*, 251−253.
(27) Campbell, M.; Sharp, D. N.; Harrison, M. T.; Denning, R. G.; Turberfield, A. J. *Nature* **2000**, *404*, 53.
(28) Xia, Y.; Gates, B.; Yin, Y.; Lu, Y. *Adv. Mater.* **2000**, *12*, 693−713.
(29) Stein, A. *Microporous Mesoporous Mater.* **2001**, *44*−*45*, 227−239 and references therein.
(30) Velev, O. D.; Jede, T. A.; Lobo, R. F.; Lenhoff, A. M. *Chem. Mater.* **1998**, *10*, 3597−3602.
(31) Yang, P. D.; Deng, T.; Zhao, D. Y.; Feng, P. Y.; Pine, D.; Chmelka, B. F.; Whitesides, G. M.; Stucky, G. D. *Science* **1998**, *282*, 2244−2246.
(32) Holland, B. T.; Abrams, L.; Stein, A. *J. Am. Chem. Soc.* **1999**, *121*, 4308−4309.
(33) Richel, A.; Johnson, N. P.; McComb, D. W. *Appl. Phys. Lett.* **2000**, *76*, 1816−1818.
(34) Yan, H.; Blanford, C. F.; Holland, B. T.; Parent, M.; Smyrl, W. H.; Stein, A. *Adv. Mater.* **1999**, *11*, 1003−1006.
(35) Velev, O. D.; Tessier, P. M.; Lenhoff, A. M.; Kaler, E. W. *Nature* **1999**, *401*, 548.
(36) Jiang, P.; Cizeron, J.; Bertone, J. F.; Colvin, V. L. *J. Am. Chem. Soc.* **1999**, *121*, 7957−7958.
(37) Yan, H.; Blanford, C. F.; Smyrl, W. H.; Stein, A. *Chem. Commun.* **2000**, *16*, 1477−1478.
(38) Wijnhoven, J. E. G. J.; Zevenhuizen, S. J. M.; Hendriks, M. A.; Vanmaekelbergh, D.; Kelly, J. J.; Vos, W. L. *Adv. Mater.* **2000**, *12*, 888−890.
(39) Yan, H.; Blanford, C. F.; Lytle, J. C.; Carter, C. B.; Smyrl, W. H.; Stein, A. *Chem. Mater.* **2001**, *13*, 4314−4321.
(40) Braun, P. V.; Wiltzius, P. *Nature* **1999**, *402*, 603−604.
(41) Vlasov, Y. A.; Yao, N.; Norris, D. J. *Adv. Mater.* **1999**, *11*, 165−169.
(42) Vlasov, Y. A.; Bo, X.-Z.; Sturm, J. C.; Norris, D. J. *Nature* **2001**, *414*, 289−293.
(43) Park, S. H.; Xia, Y. *Adv. Mater.* **1998**, *10*, 1045−1048.
(44) Park, S. H.; Xia, Y. *Chem. Mater.* **1998**, *10*, 1745−1747.
(45) Jiang, P.; Hwang, K. S.; Mittleman, D. M.; Bertone, J. F.; Colvin, V. L. *J. Am. Chem. Soc.* **1999**, *121*, 11630−11637.
(46) Johnson, S. A.; Ollivier, P. J.; Mallouk, T. E. *Science* **1999**, *283*, 963−965.
(47) Zakhidov, A. A.; Baughman, R. H.; Iqbal, Z.; Cui, C.; Khayrullin, I.; Dantas, S. O.; Marti, J.; Ralchenko, V. G. *Science* **1998**, *282*, 897−901.
(48) Zakhidov, A. A.; Khayrullin, I. I.; Baughman, R. H.; Iqbal, Z.; Yoshino, K.; Kawagishi, Y.; Tatsuhara, S. *Nanostruct. Mater.* **1999**, *12*, 1089−1095.
(49) Blanford, C. F.; Schroden, R. C.; Al-Daous, M.; Stein, A. *Adv. Mater.* **2001**, *13*, 26−29 and references therein.
(50) Deutsch, M.; Vlasov, Y. A.; Norris, D. J. *Adv. Mater.* **2000**, *12*, 1176−1180.
(51) Romanov, S. G.; Maka, T.; Sotomayor Torres, C. M.; Müller, M.; Zentel, R. *Appl. Phys. Lett.* **2001**, *79*, 731−733.
(52) Schriemer, H. P.; van Driel, H. M.; Koenderink, A. F.; Vos, W. L. *Phys. Rev. A* **2000**, *63*, 011801-1-4.
(53) Schroden, R. C.; Al-Daous, M.; Stein, A. *Chem. Mater.* **2001**, *13*, 2945−2950 and references therein.
(54) Bertone, J. F.; Jiang, P.; Hwang, K. S.; Mittleman, D. M.; Colvin, V. L. *Phys. Rev. Lett.* **1999**, *83*, 300−303.
(55) Mittleman, D. M.; Bertone, J. F.; Jiang, P.; Hwang, K. S.; Colvin, V. L. *J. Chem. Phys.* **1999**, *111*, 345.
(56) Thijssen, M. S.; Sprik, R.; Wijnhoven, J. E. G. J.; Megens, M.; Narayanan, T.; Lagendijk, A.; Vos, W. L. *Phys. Rev. Lett.* **1999**, *83*, 2730−2733.
(57) Asher, S. A.; Holtz, J.; Weissman, J.; Pan, G. S. *MRS Bull.* **1998**, *23*, 44.
(58) Míguez, H.; Mesguer, F.; López, C.; Blanco, A.; Moya, J. S.; Requena, J.; Mifsud, A.; Fornés, V. *Adv. Mater.* **1998**, *10*, 480−483.
(59) Gates, B.; Park, S. H.; Xia, Y. *Adv. Mater.* **2000**, *12*, 653−656.
(60) Lee, K.; Asher, S. A. *J. Am. Chem. Soc.* **2000**, *122*, 9534−9537.
(61) Debord, J. D.; Lyon, L. A. *J. Phys. Chem. B* **2000**, *104*, 6327−6331.
(62) Shkunov, M. N.; DeLong, M. C.; Raikh, M. E.; Vardeny, Z. V.; Zakhidov, A. A.; Baughman, R. H. *Synth. Met.* **2001**, *116*, 485−491.

als,[63,64] application of UV light to photochromic dye-filled materials,[65,66] and changes in template size[49,67−70] and angle of incidence.[11,12,33,56,71−73]

In the current report, we prepared three-dimensionally ordered macroporous materials by methods that optimized their photonic crystal properties, and we studied various methods for controlling and predicting the optical properties of these materials. Results of optical measurements were compared to theoretical predictions. A strong agreement was found between the spectral positions of the optical reflections and those predicted by the Bragg diffraction model. The pore size of these materials was found to be directly proportional to the wavelength of the optical stop band. Filling the voids of the macroporous materials with solvents of various refractive indices yielded a linear response in the shift of the spectral position of the stop band. Optical methods were utilized to calculate the average pore size of the materials, giving values very similar to those measured by scanning electron microscopy (SEM). Both Bragg theory and dynamical diffraction theory (DDT) were used to calculate the solid volume fractions, with better values obtained from DDT. The compositions of the photonic crystals, as well as the microstructures of the walls, were found to affect the optical properties of the materials. A crystallographic indexing of the optical spectrum of a polycrystalline inverse opal was performed to confirm the fcc ordering of the pores.

Experimental Section

Materials. Reagents were obtained from the following sources: tetramethoxysilane (TMOS), (3-mercaptopropyl)trimethoxysilane (MPTMS), titanium(IV) propoxide, zirconium acetate (solution in dilute acetic acid, 15−16% Zr), zirconium-(IV) propoxide (70 wt % solution in 1-propanol), HCl (37%), tetrahydrofuran (THF), methyl methacrylate (MMA), 2,2′-azobis(2-methylpropionamidine) dihydrochloride, 2-propanol, dimethylformamide (DMF), toluene, and 1,2-dibromoethane were from Aldrich; absolute ethanol was from Aaper Alcohol and Chemical Co.; methanol and acetone were from Pharmco Products Inc. All chemicals were used as received without further purification. Macroporous zirconia from alkoxide precursors was prepared according to a literature method.[17] Polystyrene sphere colloidal crystals were prepared according to a literature method.[19] The average PS sphere size was 355 ± 5 nm, as measured by SEM. Water used in all syntheses was distilled and deionized to 17.7 MΩ·cm.

Synthesis of PMMA Colloidal Crystals. Monodisperse poly(methyl methacrylate) (PMMA) spheres were synthesized using an optimized version of literature techniques[74,75] and packed into colloidal crystals. PMMA spheres were synthesized at 70−80 °C from mixtures with a typical composition of 1.6 L of water, 300−400 mL of methyl methacrylate (MMA), and 1.5 g of 2,2′-azobis(2-methylpropionamidine) dihydrochloride as an azo initiator. Water and MMA were added to a five-neck round-bottom flask, to which was attached an electric stirrer driving a glass stirring shaft with a Teflon stirrer blade, a water-cooled condenser, a pipet connected to a house supply of nitrogen gas, and a thermocouple probe attached to a temperature controller. The mixture was stirred at approximately 350 rpm, while being heated to 70−80 °C and purged with nitrogen gas. After stabilization of the temperature at an elevated level, the azo initiator was added, and the reaction was allowed to proceed for 1−2 h, producing colloidal PMMA spheres. The colloidal polymer was filtered through glass wool to remove any large agglomerates. PMMA colloidal crystals were formed by centrifuging the colloid at 1500 rpm for 24 h, decanting the water, and allowing the solid to dry for 3 days. Before being used as templates, the PMMA colloidal crystal pellets were crushed with a metal spatula to form a powder. PMMA spheres used in the syntheses of macroporous materials had diameters of 310 ± 5 nm, 375 ± 5 nm, and 425 ± 5 nm, as measured by scanning electron microscopy (SEM). In a typical synthesis, 10 g of PMMA was used to produce about 0.5−1.5 g of macroporous material.

Synthesis of Macroporous Silica. Macroporous silica was prepared by an optimized version of a literature method.[19] Samples were synthesized from mixtures with a typical composition of 6.0 mL of TMOS, 4.0 mL of methanol, 3.0 mL of water, and 1.0 mL of HCl. The reagents were added to a small vial, and the mixture was stirred at room temperature for several minutes. Dried PMMA sphere colloidal crystals were crushed to a powder and deposited in millimeter-thick layers on filter paper in a Büchner funnel. With suction applied to the Büchner funnel, the silica precursor solution was applied dropwise until it completely covered the PMMA spheres. Equal amounts, by mass, of PMMA and precursor solution were used. The composite sample was allowed to dry in air at room temperature for 24 h. The PMMA template was removed from the sample by calcination in air. In a typical calcination, the temperature was increased from ambient at a rate of 2 °C min^{-1}, stabilized at 300 °C for 2 h, increased at a rate of 2 °C min^{-1}, stabilized at 550 °C for 10 h, and then decreased to ambient temperature at a rate of 10 °C min^{-1}. The final products were colorful silica powders. Silica samples were prepared from PMMA spheres with average diameters of 310 ± 5 nm and 375 ± 5 nm, producing mean macropore sizes in silica of 265 ± 5 nm [sample SiO_2(265)] and 320 ± 5 nm [sample SiO_2(320)], respectively, as measured by SEM.

Synthesis of Macroporous Mercaptopropyl Silica. Macroporous mercaptopropyl-functionalized silica was prepared via direct synthesis by an optimized version of a literature method.[19] The sample was synthesized from a mixture of 3.0 mL of TMOS, 1.5 mL of MPTMS, 1.2 mL of water, 0.3 mL of HCl, and 3.0 mL of methanol. TMOS and MPTMS were added to a small vial and were stirred at room temperature for several minutes. Water, HCl, and methanol were mixed in a separate vial, and then this solution was added to the TMOS/MPTMS mixture. The combined solution was stirred for 3 min. This precursor was added to PS colloidal crystals and allowed to dry as described above. The PS template was removed from the sample by extraction for 5 days in a refluxing solution of 1:1 (v/v) THF and acetone. The powder product was recovered by filtration and washed with THF/acetone and then acetone. The sample was prepared from PS spheres with an average diameter of 355 ± 5 nm, producing a mean macropore size of 310 ± 5 nm [sample $MSiO_2$(310)] as measured by SEM. Elemental analysis (wt %): Si, 39; C, 21; H, 4; S, 9.

(63) Busch, K.; John, S. *Phys. Rev. Lett.* **1999**, *83*, 967−970.
(64) Yoshino, K.; Nambu, H.; Oue, T.; Shimoda, Y.; Kawagishi, Y.; Nakayama, K.; Yablonskii, S.; Uto, S.; Ozaki, M. *Mol. Cryst. Liq. Cryst.* **2000**, *347*, 339−353.
(65) Gu, Z.-Z.; Hayami, S.; Meng, Q.-B.; Iyoda, T.; Fujishima, A.; Sato, O. *J. Am. Chem. Soc.* **2000**, *122*, 10730−10731.
(66) Gu, Z.-Z.; Iyoda, T.; Fujishima, A.; Sato, O. *Adv. Mater.* **2001**, *13*, 1295−1298.
(67) Subramania, G.; Constant, K.; Biswas, R.; Sigalas, M. M.; Ho, K.-M. *Appl. Phys. Lett.* **1999**, *74*, 3933−3935.
(68) Subramanian, G.; Manoharan, V. N.; Thorne, J. D.; Pine, D. J. *Adv. Mater.* **1999**, *11*, 1261−1265.
(69) Wijnhoven, J. E. G. J.; Bechger, L.; Vos, W. L. *Chem. Mater.* **2001**, *13*, 4486−4499.
(70) Meng, Q.-B.; Fu, C.-H.; Einaga, Y.; Gu, Z.-Z.; Fujishima, A.; Sato, O. *Chem. Mater.* **2002**, *14*, 83−88.
(71) Müller, M.; Zentel, R.; Maka, T.; Romanov, S. G.; Sotomayor Torres, C. M. *Adv. Mater.* **2000**, *12*, 1499−1503.
(72) McComb, D. W.; Treble, B. M.; Smith, C. J.; De La Rue, R. M.; Johnson, N. P. *J. Mater. Chem.* **2001**, *11*, 142−148.
(73) Romanov, S. G.; Maka, T.; Sotomayor Torres, C. M.; Müller, M.; Zentel, R.; Cassagne, D.; Manzanares-Martinez, J.; Jouanin, C. *Phys. Rev. E* **2001**, *63*, 056603-1-5.
(74) Goodwin, J. W.; Ottewill, R. H.; Pelton, R.; Vianello, G.; Yates, D. E. *Br. Polym. J.* **1978**, *10*, 173−180.
(75) Zou, D.; Ma, S.; Guan, R.; Park, M.; Sun, L.; Aklonis, J. J.; Salovey, R. *J. Polym. Sci. A: Polym. Chem.* **1992**, *30*, 137−144.

Synthesis of Macroporous Titania. Macroporous titania was prepared by an optimized version of literature methods.[17−19,69] Samples were synthesized from mixtures with a typical composition of 5.0 mL of ethanol, 1.0 mL of HCl, 5.0 mL of titanium(IV) propoxide, and 2.0 mL of water. The reagents were added to a small vial in the order listed above, and the mixture was stirred at room temperature for several minutes. This precursor was added to PMMA colloidal crystals and allowed to dry as described above. The PMMA template was removed from the sample by calcination in an air/nitrogen mixture. In a typical calcination, the temperature was increased from ambient at a rate of 2 °C min^{-1}, stabilized at 300 °C for 2 h, increased at a rate of 2 °C min^{-1}, stabilized at 400 °C for 2 h, and then decreased to ambient temperature at a rate of 10 °C min^{-1}. The final products were colorful titania powders. Titania samples were prepared from PMMA spheres with average diameters of 310 ± 5 nm and 375 ± 5 nm, producing mean macropore sizes in titania of 250 ± 5 nm [sample TiO_2(250)] and 310 ± 5 nm [sample TiO_2(310)], respectively, as measured by SEM.

Synthesis of Macroporous Zirconia. Macroporous zirconia was prepared by an optimized version of a literature method.[21] Samples were synthesized from mixtures with a typical composition of 6.0 mL of methanol and 6.0 mL of zirconium acetate (solution in dilute acetic acid). The reagents were added to a small vial and were stirred at room temperature for several minutes. This precursor was added to PMMA colloidal crystals and allowed to dry as described above. The PMMA template was removed from the sample, and the zirconium acetate was converted to zirconia by calcination in an air/nitrogen mixture. In a typical calcination, the temperature was increased from ambient at a rate of 2 °C min^{-1}, stabilized at 300 °C for 2 h, increased at a rate of 2 °C min^{-1}, stabilized at 450 °C for 2 h, and then decreased to ambient temperature at a rate of 10 °C min^{-1}. The final products were brightly colored zirconia powders. Zirconia samples were prepared from PMMA spheres with average diameters of 310 ± 5 nm, 375 ± 5 nm, and 425 ± 5 nm, producing mean macropore sizes in zirconia of 200 ± 5 nm [sample ZrO_2(200)], 250 ± 5 nm [sample ZrO_2(250)], and 285 ± 5 nm [sample ZrO_2(285)], respectively, as measured by SEM.

Characterization. Diffuse-reflectance UV−vis spectra were obtained on a Hewlett-Packard 8452A diode array spectrophotometer equipped with a Labsphere RSA-HP-84 reflectance spectroscopy accessory. Spectra were obtained for randomly oriented bulk powder samples. Reflectance data were converted to $f(R_\infty)$ values using the Kubelka−Munk equation. Scanning electron microscopy (SEM) images were obtained on a Hitachi S-800 scanning electron microscope operating at 4 kV. Samples for SEM were dusted on an adhesive conductive carbon disk attached to an aluminum mount and were coated with Pt prior to examination. Polymer sphere diameters and inverse opal pore sizes were determined from the SEM images. An Abbe refractometer was used to determine the refractive indices of macroporous silica and mercaptopropyl silica by solvent refractive index matching. Powder X-ray diffraction (XRD) analyses were performed on a Siemens D5005 wide-angle XRD spectrometer with Cu Kα radiation operating at 40 kV and 45 mA. Phases and grain sizes were determined by using the JADE 5 program. Elemental analyses were performed for Si at the Geochemical Lab, University of Minnesota, Minneapolis, MN, and for C, H, and S at Atlantic Microlab Inc., Norcross, GA.

Results and Discussion

Synthesis of Macroporous Materials. The composition and microstructure of the walls of macroporous materials affect their photonic crystal properties. As a result, careful control of the synthetic conditions was required to produce materials with brightly colored optical reflections. Each of the four types of macroporous materials prepared in this report required different types of precursors and processing conditions to optimize their photonic crystal properties. Alkoxides were used as precursors for silica and titania, whereas zirconia required the use of zirconium acetate to yield materials with maximized optical reflections. The best results for silica and titania were obtained when TMOS and titanium(IV) propoxide were used as the respective precursors. Both of these precursors are moisture-sensitive, and titanium(IV) propoxide is very viscous, so the alkoxides were diluted with alcohols to decrease reactivity and increase penetration through the polymer template. Addition of an acid to the alkoxide precursors decreased the rates of condensation, preventing premature metal oxide precipitation upon exposure to air. The addition of an acid was especially important for forming ordered titania, because titanium alkoxides are very reactive and undergo rapid condensation when exposed to moisture. Zirconium alkoxides are even more reactive and water-sensitive than those of titanium, making zirconium acetate the preferred precursor for zirconia because of its ease of handling and lower reactivity.

In addition to the appropriate choice of precursors, it was necessary to tailor the template removal conditions for each type of material to maximize the optical reflections. Extraction of the PS template in a refluxing THF/acetone solution was the method of choice for producing macroporous mercaptopropyl silica to preserve the organic groups. For the metal oxides, on the other hand, calcination was the preferred method of template removal. The optimum calcination conditions varied for the different types of oxides. Higher temperatures, longer heating times, and an atmosphere of air were used for removal of PMMA from silica. In contrast, lower temperatures, shorter heating times, and a mixed nitrogen/air atmosphere was required to produce macroporous titania and zirconia with strong photonic crystal properties (i.e., brightly colored samples). The milder conditions required for titania and zirconia, compared to silica, are related to their respective wall microstructures. Because the silica samples have amorphous walls, higher temperatures and longer heating times were beneficial as they aided further condensation of the walls. In contrast, titania and zirconia have nanocrystalline microstructures in which small grains are fused together to form the larger wall structure.[76] In these structures the grain size must be very small in comparison to the void dimensions to have the uniform periodicity required for photonic crystal behavior. As a consequence of this crystalline microstructure, milder template removal techniques were required to control grain growth and keep the morphology of the macroporous structure closer to that of an fcc structure. Optimized synthetic conditions allowed the production of macroporous titania and zirconia samples with very limited grain growth. The macroporous titania samples had the anatase phase, with average grain sizes of 10 nm (as determined from powder X-ray diffraction), whereas the zirconia samples were tetragonal, with average grain sizes of 1−2 nm. Because of the limited grain growth of these samples, they exhibited very prominent photonic crystal properties, especially with respect to their bright colors.

(76) Blanford, C. F.; Yan, H.; Schroden, R.; Al-Daous, M.; Stein, A. *Adv. Mater.* **2001**, *13*, 401−407.

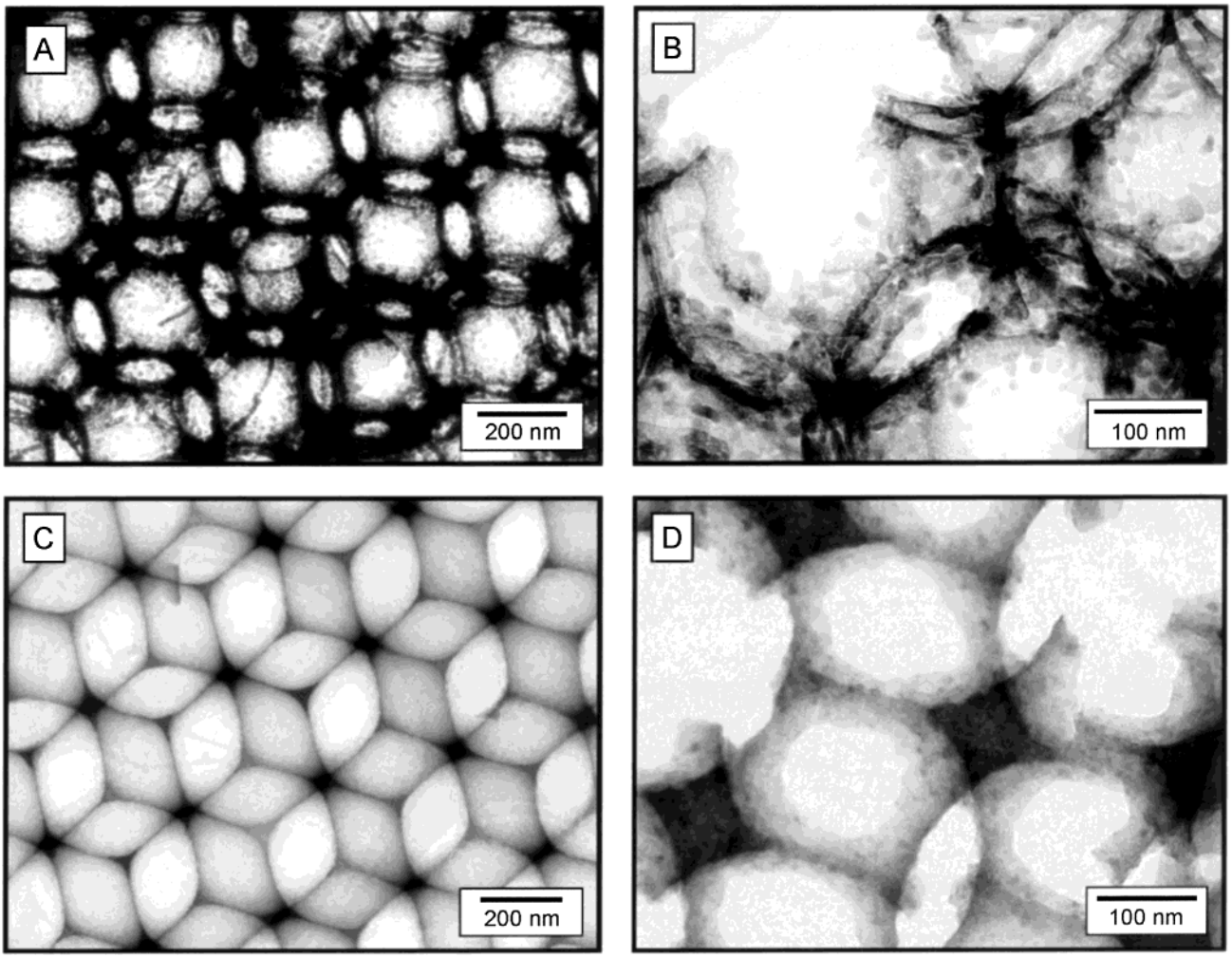

Figure 1. Transmission electron microscopy (TEM) images of three-dimensionally ordered macroporous zirconia prepared from (A, B) zirconium(IV) propoxide and (C, D) zirconium acetate. The dark regions correspond to the wall structures, and the lighter regions to void spaces. An increased ordering of the wall structure is observed for the sample in C and D because of limited growth of the nanocrystalline grains (1−2 nm) compared to the sample in A and B, which has larger grains (28 nm). As a result of this difference in microstructure, materials prepared from the alkoxides appear visibly white, whereas those prepared from the acetate appear brightly colored.

The importance of careful control of the synthetic conditions in the production of photonic crystals is demonstrated by transmission electron microscopy (TEM) images of macroporous zirconia (Figure 1). The dark regions in the images represent the solid framework, and the light regions represent the voids. The top images (Figure 1A and B) are of a sample prepared from an alkoxide precursor, whereas the bottom sample (Figure 1C and D) was prepared from the acetate. Zirconia prepared from the alkoxide had an average grain size of 28 nm (as determined by powder X-ray diffraction), compared to the 1−2-nm grain size for the sample prepared from the acetate. This difference in the microstructures of the two zirconia samples resulted in the different visual appearances of the samples. The macroporous zirconia sample with large grains appeared white as a result of random light scattering from the grains, whereas the sample with smaller grains was brightly colored as a result of Bragg diffraction of light from the highly ordered periodic structure and less random scattering.

Scanning electron microscopy (SEM) images of representative samples of macroporous silica, mercaptopropyl silica, titania, and zirconia are presented in Figure 2. The lighter regions in the images represent the solid framework, and the darker circles are the "air spheres" that were previously occupied by polymer spheres. Former contact points between neighboring polymer spheres appear as windows between the macropores. Small openings are present in the walls of the macropores of mercaptopropyl silica at the center of each triangular intersection of three air spheres. The presence of these voids has been shown to enhance the photonic crystal properties of inverse opals.[77] Similar openings have also been observed for other compositions of inverse opal materials.[18,33,47,69] This is likely due to the adherence of the precursor to the polystyrene template,[78] resulting in a surface-templated[47] filling in which condensation of the walls occurred at the surface of the spheres, blocking the introduction of additional precursor solution into the intersections. The absence of these features in the silica, titania, and zirconia samples (templated by PMMA) suggests that a volume-templated[47] filling occurred in which the precursors

(77) Busch, K.; John, S. *Phys. Rev. E* **1998**, *58*, 3896−3908.
(78) Jiang, P.; Bertone, J. F.; Colvin, V. L. *Science* **2001**, *291*, 453−457.

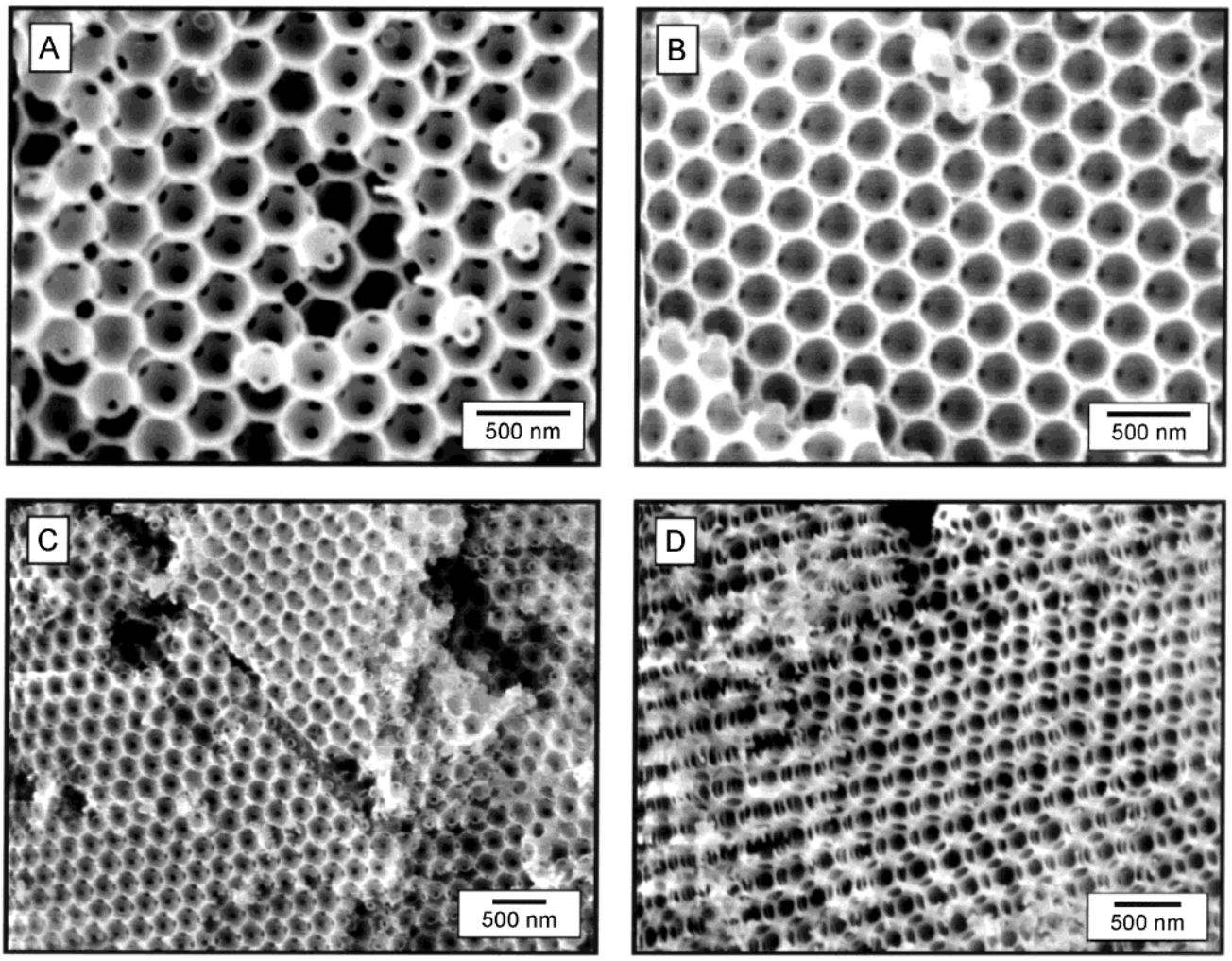

Figure 2. Scanning electron microscopy (SEM) images of three-dimensionally ordered macroporous (A) silica, (B) mercaptopropyl silica, (C) titania, and (D) zirconia. The white skeletal structures in these images are the walls of the macroporous materials, and the darker spherical regions are void spaces. Windows between macropores can be clearly seen in A at the positions of former contact points between polymer spheres. Small openings at the center of each triangular intersection of three macropores in B are indicative of surface templating due to adherence of the precursor to the PS template. The absence of these openings in the other samples (templated by PMMA) is indicative of volume templating.

completely filled the volume between the spheres prior to condensation and/or crystallization. The shrinkage observed from the diameter of the original polymer sphere templates to the spacing between the pores was about 15% for silica, 13% for mercaptopropyl silica, 18% for titania, and 34% for zirconia.

The colloidal crystals used as templates for the macroporous materials were intentionally crushed so that powder products could be obtained. This process limited the size of ordered domains and increased the number of defects in the structure. Although such defects have been calculated to close a photonic band gap,[79,80] ordered structures with as few as eight layers have been demonstrated to exhibit 99% reflectivity.[26] In general, the bright colors of the samples reported here were far more sensitive to the grain size of the walls than to the size of the ordered domains.

Theoretical Basis of Optical Properties. Each type of wall material forming the structures of the inverse opals described in the current report does not absorb in the visible spectrum. Nevertheless, the materials appear brightly colored. Like natural opals, the polymer colloidal crystal templates used to form the macroporous materials in this report have microstructures consisting of a close-packed arrangement of spheres. The ordered arrangement of the colloidal crystal is transferred to the inorganic inverse replica through the templating process, producing a close-packed arrangement of air spheres in an inorganic matrix. As a result of optical diffractions from the crystal lattice planes, the macroporous materials exhibit colorful reflections similar to those observed in natural opals.

An approximate expression for the spectral positions of the stop bands for an inverse opal photonic crystal can be calculated by a modified version of Bragg's law, combined with Snell's law to account for the reduced angle with respect to the normal that light travels upon entering a medium of a higher refractive index[49,53]

$$\lambda = \frac{2d_{hkl}}{m}\sqrt{{n_{\mathrm{avg}}}^2 - \sin^2\theta} \qquad (1)$$

where λ is the wavelength of the stop band minimum

(79) Li, Z.-Y.; Zhang, Z.-Q. *Phys. Rev. B* **2000**, *62*, 1516−1519.
(80) Li, Z.; Zhang, Z. *Adv. Mater.* **2001**, *13*, 433−436.

(i.e., the wavelength of maximum reflected intensity), m is the order of Bragg diffraction, n_{avg} is the average refractive index of the macroporous material, and θ is the angle measured from the normal to the planes. Because the optical reflectance measurements made in this report were on bulk powdered (randomly oriented) photonic crystal samples, the spectra display stop band minima at the calculated values for normal incidence ($\theta = 0°$), and the angle dependence of the stop band position is lost. Dropping the angle dependence from eq 1 yields stop band positions that are proportional to both the interplanar spacing and the average refractive index of the macroporous material

$$\lambda = \frac{2d_{hkl}}{m} n_{avg} \tag{2}$$

The arrangement of the pores in macroporous materials, and of the spheres in their colloidal crystal templates, is widely regarded to be face-centered-cubic (fcc).[28] The apparent preference of spherical colloidal particles to self-assemble into the fcc arrangement instead of the hexagonal-close-packed (hcp) arrangement has been suggested to be a result of a more favorable entropy for fcc formation.[81,82] The fcc ordering of macroporous materials has recently been confirmed by small-angle X-ray diffraction[69] and tilting in the TEM images.[19] For an fcc structure, nonzero reflections (or photonic crystal stop bands) are predicted to occur for either all even or all odd h, k, l indices. Therefore, if the pore ordering is fcc, stop bands should exist for reflections from the (hkl) planes (111), (200), (220), (311), etc. For "polycrystalline" photonic crystals, in which a random orientation of the crystal planes exists, multiple stop bands should be present in a single spectrum. However, most spectra of macroporous materials reported to date have exhibited stop bands in the UV−visible region from only one or two sets of planes.

A definitive experimental determination of the pore ordering in macroporous materials could be made from an optical spectrum if multiple stop bands could be indexed to different sets of planes in a manner analogous to the indexing of powder X-ray diffraction patterns to determine the pore arrangement of mesoporous silicates.[83,84] For a macroporous material with an fcc structure, the interplanar spacing (d_{hkl}) for each set of (hkl) diffraction planes would relate to the pore spacing (D) and unit cell parameter (a) by the equation

$$d_{hkl} = \frac{a}{\sqrt{h^2 + k^2 + l^2}} = \frac{D\sqrt{2}}{\sqrt{h^2 + k^2 + l^2}} \tag{3}$$

From eqs 2 and 3, it can be seen that the wavelengths (λ) of the stop bands are inversely proportional to $(h^2 + k^2 + l^2)^{1/2}$. Therefore, structures with an fcc arrangement of pores would have stop band wavelengths from the (200), (220), and (311) planes with ratios to the (111) stop band wavelength of $\sqrt{3}/\sqrt{4}$, $\sqrt{3}/\sqrt{8}$, and $\sqrt{3}/\sqrt{11}$, or 0.866, 0.612, and 0.522, respectively.

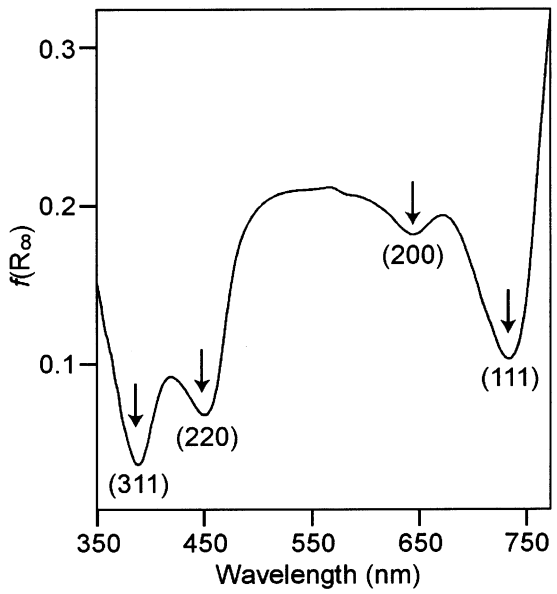

Figure 3. Diffuse-reflectance UV−vis spectrum of a powdered sample of three-dimensionally ordered macroporous mercaptopropyl silica filled with 2-propanol. This polycrystalline photonic crystal exhibits stop bands (optical reflections) corresponding to (hkl) planes with all odd or all even h, k, l indices. The stop band minima (marked with arrows) correspond to diffraction from the (111), (200), (220), and (311) sets of planes.

Whereas the spectra of most samples in the current work exhibited two stop bands in the UV−visible region, the macroporous mercaptopropyl-functionalized silica sample exhibited four stop bands when filled with 2-propanol. The diffuse-reflectance UV−vis spectrum of this sample, in which the minima correspond to optical stop bands, is given in Figure 3. The stop band wavelengths of this sample are observed at 734, 644, 450, and 388 nm. The ratios of the lower-wavelength stop bands to the stop band at 734 nm (having values of 0.877, 0.613, and 0.529) are in very close agreement with the theoretical values presented above. We can, therefore, conclude that the stop bands are caused by reflections from the (111), (200), (220), and (311) sets of planes, respectively, and that the macroporous material has an fcc arrangement of pores. To the best of our knowledge, this is the first report of the crystallographic indexing of an optical spectrum of a polycrystalline inverse opal exhibiting reflections from four crystal planes.

To estimate the wavelengths of the stop bands of inverse opal photonic crystals, the effective medium approximation[85,86] ($n_{avg} = \sum_i n_i\phi_i$, where n_i and ϕ_i are the refractive index and volume fraction of component i in the material), which assumes that the average refractive index of a material is a weighted sum of the refractive indices of its components, can be combined with eq 2 to yield

$$\lambda = \frac{2d_{hkl}}{m} [\phi n_{walls} + (1 - \phi) n_{voids}] \tag{4}$$

where ϕ is the volume fraction of the solid wall material, n_{walls} is the refractive index of the wall material (e.g.,

(81) Woodcock, L. V. *Nature* **1997**, *385*, 141−143.
(82) Bolhuis, P. G.; Frenkel, D.; Mau, S.-C.; Huse, D. A. *Nature* **1997**, *388*, 235−236.
(83) Kresge, C. T.; Leonowicz, M. E.; Roth, W. J.; Vartuli, J. C.; Beck, J. S. *Nature* **1992**, *359*, 710−712.
(84) Beck, J. S.; Vartuli, J. C.; Roth, W. J.; Leonowicz, M. E.; Kresge, C. T.; Schmitt, K. D.; Chu, C. T.-W.; Olson, D. H.; Sheppard, E. W.; McCullen, S. B.; Higgins, J. B.; Schlenker, J. L. *J. Am. Chem. Soc.* **1992**, *114*, 10834−10843.

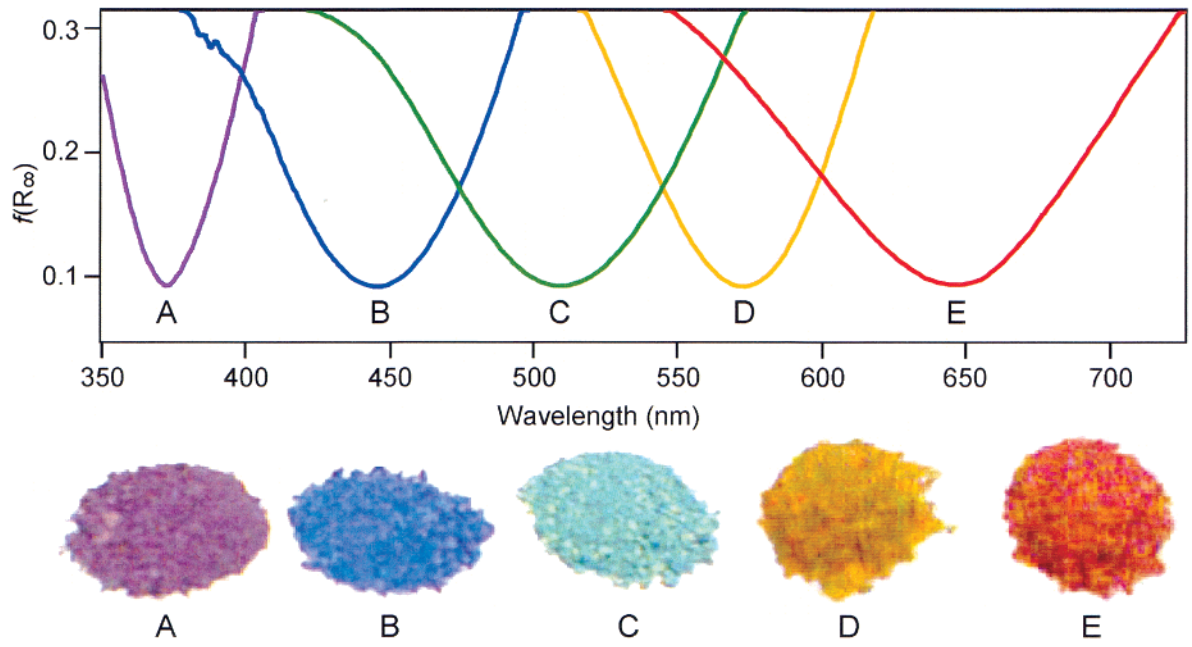

Figure 4. Inverse opal photonic crystal powders of zirconia with optical reflections spanning the colors of the visible spectrum. Diffuse-reflectance UV−vis spectra (top) and photographs (bottom) of three-dimensionally ordered macroporous zirconia powders demonstrating the effects of pore size and the presence of solvent in the pores on the color of the samples. The stop band minima correspond to the wavelengths of maximum reflection. (A) ZrO_2(200), (B) ZrO_2(250), (C) ZrO_2(285), (D) ZrO_2(250) filled with methanol, (E) ZrO_2(285) filled with methanol. Increasing the pore size or filling the pores with solvents results in an increase in the wavelength of light reflected by the photonic crystal.

$n_{silica} = 1.455$, $n_{zirconia} = 2.13$, $n_{titania} = 2.50$), and n_{voids} is the refractive index of the void spaces. A solid volume fraction of 26% would be predicted for an exact inverse replica of close-packed spheres. However, the actual solid volume fraction is often much lower than 26% as a result of dilution of the precursors to aid template infiltration, as well as condensation of the precursors.

The Bragg's law approximation is not exact because it neglects attenuation of the incident beam and assumes identical contributions from each lattice plane.[87] Corrections to Bragg's law have been made by using dynamical diffraction theory (DDT), which considers coupling of the incident and diffracted waves due to strong scattering.[87,88] The DDT prediction for the diffracted wavelength (λ_D) at normal incidence is related to the Bragg prediction (λ_B) according to the relationship[89]

$$\lambda_D = \lambda_B\left(1 + \frac{\psi}{2}\right) \tag{5}$$

where ψ is a parameter that can be estimated by[85,90]

$$\psi = 3\phi\frac{r^2 - 1}{r^2 + 2} \tag{6}$$

where r is the ratio of the refractive indices of the walls and the voids (i.e., $r = n_{walls}/n_{voids}$). The DDT approximation for the position of the stop bands for inverse opal photonic crystals can be calculated by combining eqs 4 and 5

$$\lambda = \frac{2d_{hkl}}{m}[\phi n_{walls} + (1 - \phi)n_{voids}]\left(1 + \frac{\psi}{2}\right) \tag{7}$$

Tuning the Colors. The spectral positions of the stop bands of inverse opal photonic crystals (i.e., the wavelengths of maximum optical reflection) can be varied in a predictable manner by altering certain variables in eq 4, such as the pore size and the refractive index of the void spaces. For the macroporous materials described in this report, reflections from the (111) set of planes dominated the optical properties, specifically the color, of the materials. Because the stop band wavelength is directly proportional to the pore size, the color of the macroporous materials can be shifted to higher-wavelength colors simply by increasing the size of the polymer sphere templates used in the preparation of the samples, resulting in larger pore sizes. In addition, filling the voids of the macroporous samples with a solvent allows the position of the stop band to be systematically shifted to higher wavelengths.[10,11,49,62]

A demonstration of these color-tuning techniques is given in Figure 4 for samples of macroporous zirconia. Zirconia samples with 200-, 250-, and 285-nm pores give optical reflections at 374, 446, and 510 nm, resulting in powders that appear violet, blue, and green, respectively. The addition of methanol to the two larger-pore zirconia samples yields materials with optical reflections at 572 and 646 nm, changing the colors of the powders to yellow-orange and red, respectively. These color changes are reversible, with reversion to the original colors occurring a few minutes after wetting, following

(85) Vos, W. L.; Sprik, R.; van Blaaderen, A.; Imhof, A.; Lagendijk, A.; Wegdam, G. H. *Phys. Rev. B* **1996**, *53*, 16231−16235.
(86) Romanov, S. G.; Maka, T.; Torres, C. M. S.; Müller, M.; Zentel, R. *J. Lightwave Technol.* **1999**, *17*, 2121−2127.
(87) Liu, L.; Li, P.; Asher, S. A. *J. Am. Chem. Soc.* **1997**, *119*, 2729−2732.
(88) Rundquist, P. A.; Photinos, P.; Jagannathan, S.; Asher, S. A. *J. Chem. Phys.* **1989**, *91*, 4932−4941.
(89) Zachariasen, W. H. *Theory of X-ray Diffraction in Crystals*; John Wiley and Sons: New York, 1946.
(90) Pan, G.; Sood, A. K.; Asher, S. A. *J. Appl. Phys.* **1998**, *84*, 83−86.

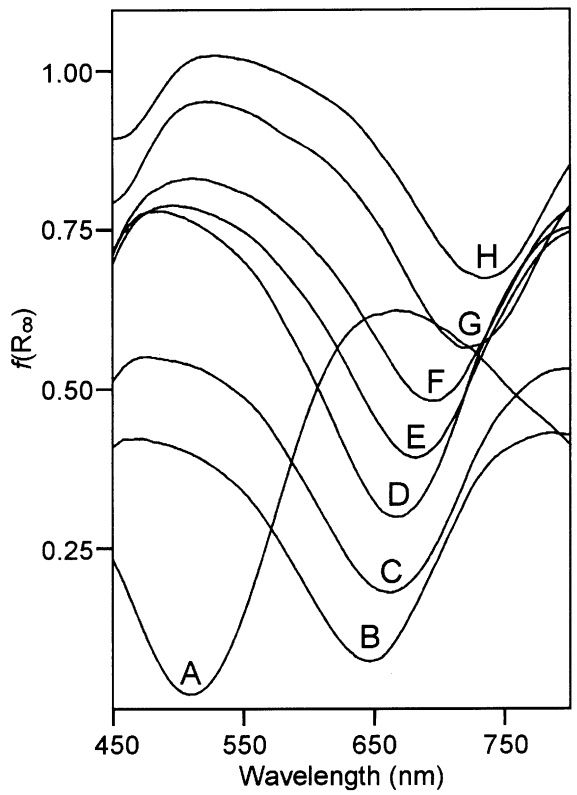

Figure 5. Diffuse-reflectance UV−vis spectra of ZrO_2(285) with voids empty and filled with fluids of various refractive indices. Spectrum with filling fluid and refractive index: (A) air, $n = 1.000$; (B) methanol, $n = 1.329$; (C) ethanol, $n = 1.360$; (D) 2-propanol, $n = 1.377$; (E) THF, $n = 1.407$; (F) DMF, $n = 1.431$; (G) toluene, $n = 1.496$; (H) 1,2-dibromoethane, $n = 1.538$. The spectral position of the stop band shifts to higher wavelengths as the refractive index of the filling fluid increases. The spectra are vertically offset for clarity.

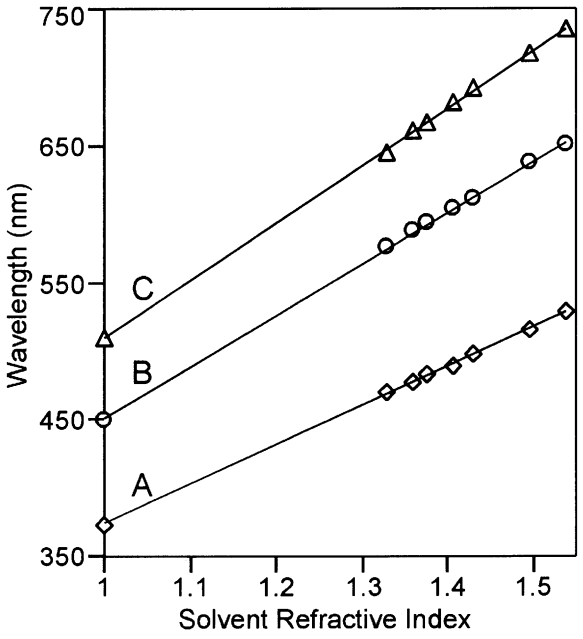

Figure 6. Plots illustrating the change in the spectral position of the stop band minimum corresponding to diffraction from the (111) sets of planes upon filling the pores of the macroporous zirconia samples [with pore sizes of (A) 200, (B) 250, and (C) 285 nm] with fluids of increasing refractive index. Macroporous materials with larger pore sizes gave longer-wavelength reflections and a greater shift in the stop band position upon solvent filling. Slopes of the linear least-squares fits of the data indicate shifts of (A) 288, (B) 377, and (C) 420 nm per unit increase in the refractive index.

evaporation of the solvent. It is noteworthy that the chemical compositions of all of the macroporous zirconia samples are identical and that zirconia does not absorb light in the visible spectral region. The origin of the observed colors of the inverse opal materials is entirely from diffraction of light from the periodic arrangement of the macroporous structure. The current materials differ from those described in previous reports of colorful reflections from macroporous thin films in that these materials are bulk powders that exhibit striking colors. This aspect might allow the use of these materials in applications such as colorful pigments.

The shift in the position of the stop bands to higher wavelengths upon filling of the void spaces of macroporous materials with solvents is greater for larger values of the solvent refractive index. This relationship was examined by filling the macroporous samples with a group of solvents that span a range of refractive indices. The fluids used to fill the pores were air ($n = 1.000$), methanol ($n = 1.329$), ethanol ($n = 1.360$), 2-propanol ($n = 1.377$), THF ($n = 1.407$), DMF ($n = 1.431$), toluene ($n = 1.496$), and 1,2-dibromoethane ($n = 1.538$). The diffuse-reflectance UV−vis spectra of fluid-filled samples of ZrO_2(285) are displayed in Figure 5. The spectra are vertically offset for clarity, and they exhibit a systematic increase in the stop band wavelength with the solvent refractive index. Diffuse-reflectance UV−vis spectra for the other samples have a similar appearance.

The position of the stop band varies in a linear manner with the refractive index of the fluid filling its pores. This result follows the Bragg's law approximation, which can be seen by rearranging eq 4 to give a linear expression for the wavelength (λ) of the stop band versus the solvent (or air) refractive index ($n_{solvent}$)

$$\lambda = \frac{2d_{hkl}}{m}\phi n_{walls} + \frac{2d_{hkl}}{m}(1 - \phi)n_{solvent} \qquad (8)$$

Plots of the wavelengths of the stop band minima versus the refractive index of the pore-filling fluid are given in Figure 6 for the three macroporous zirconia samples. In each case, a linear least-squares fit of the data gave a strong correlation between λ and $n_{solvent}$. All samples in this report gave linear fits of λ versus $n_{solvent}$ with R^2 values greater than 0.995. It can be seen from the plots in Figure 6 that larger pore sizes gave longer-wavelength reflections and a steeper response to the change in the stop band position by solvent filling. The slopes of the curves showed that the position of the stop bands shifted by approximately 288, 377, and 420 nm per unit increase in the refractive index for the ZrO_2(200), ZrO_2-(250), and ZrO_2(285) samples, respectively. These data are summarized in Table 1 for all of the macroporous materials studied in this report.

Plots of λ versus $n_{solvent}$ for reflections from a given (hkl) plane allow the solid fraction (ϕ) and the pore spacing (D) to be calculated[49] from the slope and

Table 1. Summary of Theoretical and Experimental Results[91]

sample	SiO_2 (265)	SiO_2 (320)	$MSiO_2$ (310)	ZrO_2 (200)	ZrO_2 (250)	ZrO_2 (285)	TiO_2 (250)	TiO_2 (310)
sphere size,[a] nm	310	375	355	310	375	425	310	375
D (SEM),[b] nm	265	320	310	200	250	285	250	310
D (Bragg),[c] nm	263	318	316	201	252	283	252	309
ϕ (Bragg),[d] %	8.7	4.5	24.7	12.3	8.5	9.2	7.0	8.9
ϕ (DDT),[e] %	5.7	2.3	12.4	6.5	4.5	4.8	3.8	4.8
ϕ (exp),[f] %	6.7	7.0	10.8	5.8	4.7	5.0	2.3	2.2
wt %[g]	7.9	8.2	14.0	7.3	6.6	7.1	4.1	4.2
M[h]	392	496	389	288	377	420	383	459
B[i]	54	34	196	86	74	90	72	112
n_{walls}[j]	1.455	1.455	1.534	2.13	2.13	2.13	2.50	2.50
m[k]	1	1	1	1	1	1	1	1
λ (111),[l] nm	445	530	585	374	446	510	454	572

[a] Diameter of the polymer sphere template as measured by SEM. [b] Pore size as measured by SEM. [c] Pore size calculated by the Bragg diffraction model using eq 9. [d] Solid volume fraction calculated by the Bragg diffraction model using eq 9. [e] Solid volume fraction calculated by the DDT. [f] Experimental solid volume fraction determined from the mass loss during template removal, the densities of the walls and polymer template (SiO_2, $d = 2.2$; $MSiO_2$, $d = 2.2$; ZrO_2, $d = 5.6$; TiO_2, $d = 3.84$; PMMA, $d = 1.12$; PS, $d = 1.05$), and the structural shrinkage. [g] Weight percentage of solid remaining after removal of the polymer template by calcination or solvent extraction. [h] Slope of the linear least-squares fit of the stop band wavelength versus the refractive index of the fluid filling the pores. [i] Intercept of the linear least-squares fit of the stop band wavelength versus the refractive index of the fluid filling the pores. [j] Refractive index of the walls of the macroporous materials. Experimental values were used for silica and mercaptopropyl silica, and literature estimates were used for titania and zirconia. [k] Order of Bragg reflection. [l] Wavelength of the stop band [position of maximum reflectance corresponding to diffraction from the (111) sets of planes] of the dry samples.

intercept of the linear least-squares fit by the equations

$$\phi = \frac{B}{Mn_{walls} + B}$$

$$D = \frac{m(Mn_{walls} + B)\sqrt{h^2 + k^2 + l^2}}{2\sqrt{2}n_{walls}} \qquad (9)$$

where M is the slope and B is the intercept. The benefit of the calculation of these parameters via optical methods is that the values are averaged over the entire sample, whereas pore size measurements made by SEM are averaged over a finite number of measurements and the solid fraction cannot be measured directly by SEM. For all of the samples studied in this report, excellent agreement was obtained between physical measurements and predictions made by the Bragg diffraction model. For example, the measured (and calculated) values of the pore sizes of the three macroporous zirconia samples were 200 (201), 250 (252), and 285 (283) nm. Similarly strong agreements were found for all other samples. These and other relevant data for all samples are summarized in Table 1.

(91) For the calculations listed in the Table 1, the common literature values of 2.50 and 2.13 were used for the refractive indices of titania and zirconia, respectively. Although the refractive index of the nanocrystalline walls is almost certainly lower than bulk values, this has little effect on the calculations. This result arises from the low solid fraction of the materials, which minimizes the contribution of the wall material to the average refractive index. Using TiO_2(250) as an example, pore spacings of 257, 252, and 249 nm are calculated from eq 9 when refractive index values of 2.0, 2.5, and 3.0, respectively, are inserted for titania. These values are in close agreement with each other and with the SEM measurement of 250 nm.

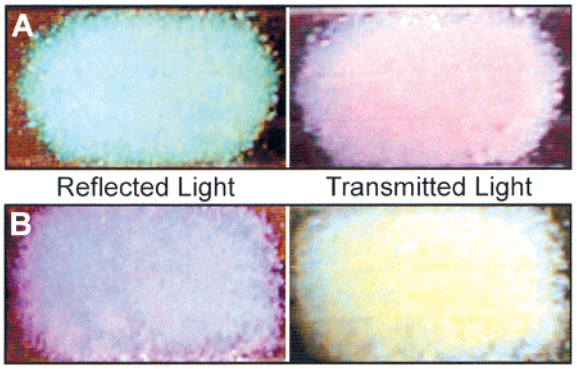

Figure 7. Photographs of three-dimensionally ordered macroporous silica powders demonstrating an optical filtering behavior in which complementary colors are observed in transmitted and reflected light. (A) SiO_2(320) observed in reflected (left) and transmitted (right) light. (B) SiO_2(265) observed in reflected (left) and transmitted (right) light. Stop bands at 530 nm for SiO_2(320) and 445 nm for SiO_2(265) give the materials green and blue appearances in reflected light and pink and yellow appearances in transmitted light, respectively.

Because the solid volume fraction cannot be determined directly by SEM, results calculated from eq 9 were compared to values of the "experimental" solid fraction calculated from the mass loss during template removal, the densities of the walls and polymer template, and the structural shrinkage. DDT was also compared to Bragg theory in the estimation of the solid volume fraction. For these calculations, the values n_{walls} and D were fixed, and ϕ was optimized numerically using the values calculated from eq 9 as seeds. Solid volume fractions calculated by the DDT were typically in closer agreement with the experimental values than were the Bragg predictions.

Optical Filtering. The microstructure of the walls of the macroporous materials affects their optical properties. The presence of nanocrystalline grains in the walls of titania and zirconia leads to an opaque appearance because of scattering of light from the grains. The apparent colors of these samples remain the same regardless of the viewing conditions. The macroporous silica samples, however, have amorphous walls and appear relatively transparent. As a result, the macroporous silica materials exhibit an optical filtering behavior (shown in Figure 7). These photographs demonstrate how powdered samples of SiO_2(265) and SiO_2(320) held between glass microscope slides change colors when observed in reflected or transmitted light. In reflected light, the color corresponding to wavelengths inhibited from passing through the photonic crystal is observed. In transmitted light, the complementary color, consisting of light wavelengths that are allowed to pass through the photonic crystal, is observed. The respective stop bands corresponding to diffraction from the (111) set of planes for samples SiO_2(265) and SiO_2(320) are observed at 445 and 530 nm, giving blue and green appearances in reflected light and yellow and pink appearances in transmitted light, respectively.

Conclusion

Synthetic methods have been presented for the preparation of inverse opal photonic crystals that exhibit

tailorable optical properties. Optimization of the synthetic procedures yielded materials with brightly colored reflections. The spectral position of the optical stop bands of these materials was found to be in strong agreement with theoretical predictions based on Bragg diffraction from the lattice planes of the three-dimensionally ordered macroporous structure. The color of the materials was predictably altered by changing the pore spacing and infiltrating the pores with fluids of various refractive indices. The wavelengths of light reflected by the photonic crystals were found to be directly proportional to their pore sizes. Addition of solvents to the pores of the macroporous materials resulted in a linear shift in the spectral position of the stop band with respect to the refractive index of the filling fluid. The use of optical measurements to calculate the pore size of macroporous materials was found to be an effective method for determining the statistically averaged pore size of the material. The microstructure of the walls of the inverse opals was found to affect the visible appearance of the materials. Macroporous materials with nanocrystalline walls exhibited colors corresponding to the wavelengths of their photonic stop band regardless of the viewing conditions. In contrast, macroporous materials with amorphous walls exhibited the color of the stop band wavelengths when viewed in reflected light and the complementary color when observed in transmitted light. A crystallographic indexing of the optical spectrum of a macroporous material confirmed that the pores were arranged in an fcc structure. The compositional flexibility of these syntheses, the remarkable colors of the materials and striking color changes that occur upon filling with different fluids, and the powdered nature of the macroporous materials presented here suggest that they can be applied in the areas of chemical sensors, optical filters, or photonic pigments. The solvent-filling approach might also be used for switching or tuning a photonic band gap by shifting it in to or out of a desired spectral region.

Acknowledgment. We thank the U.S. Army Research Laboratory and the U.S. Army Research Office under Contract/Grant DAAD 19-01-1-0512, the National Science Foundation (DMR-9701507), the MRSEC program of the NSF (DMR-9809364), and the David and Lucile Packard Foundation for support of this research. We thank Sergey Sokolov, Hongwei Yan, Justin Lytle, and Thuy Truong for experimental assistance.

CM020100Z